Chemical
Science

This article can be cited before page numbers have been issued, to do this please use: R. Li, S. Xie, Y. Li, X. Wang, S. Liu, J. Qian, Y. Zhang, L. Jiang, Z. Cao, Z. Yan, X. Wan, Z. Yang, L. Zou and W. Zhang, *Chem. Sci.*, 2025, DOI: 10.1039/D5SC01884F.

ROYAL SOCIETY
OF CHEMISTRY

rsc.li/chemical-science

View Article Online
DOI: 10.1039/D5SC01884F

# Modulation of electronic structure of nickel selenide via iron doping for energy-saving hydrogen production coupled with sulfion upgrading

Received 00th January 20xx,
Accepted 00th January 20xx

DOI: 10.1039/x0xx00000x

Shuixiang Xie,[a,1] Xiaojun Wang,[a,1] Yuhuan Li,[a] Shijie Liu,[a] Jiahui Qian,[a] Yuhan Zhang,[a] Linling Jiang,[a] Zhe Cao,[a] Zhenhao Yan,[a] Xiaoyu Wan,[a] Zhaohang Yang,[a] Longhua Zou,*[b] Wei Zhang,*[a] and Rui-Qing Li*[a]

Hybrid water electrolysis is a promising approach to achieve energy-saving hydrogen ($H_2$) generation by replacing oxygen evolution reaction with thermodynamically advantageous sulfion oxidation reaction (SOR). Herein, we design iron-modified nickel selenide nanosheet arrays (Fe-Ni$_{0.85}$Se) as a bifunctional hydrogen evolution reaction (HER) and SOR electrocatalyst to simultaneous facilitate $H_2$ production and convert sulfion into valuable sulfur product. The Fe-Ni$_{0.85}$Se needs low overpotential of 114 mV for HER and working potential of 0.340 V for anodic SOR to attain 10 mA cm$^{-2}$. Moreover, the two-electrode hybrid electrolysis cell employing Fe-Ni$_{0.85}$Se as cathode and anode requires small voltage of 0.439 V at 10 mA cm$^{-2}$, which greatly reduces operation voltage by 1.186 V compared with overall water splitting, realizing energy-saving $H_2$ production and high value-added sulfur source. The theoretical calculations verify that the Fe modification can accelerate water dissociation, optimize the adsorption behavior of hydrogen adsorption and sulfion, and promote conversion process of sulfur intermediates. This work offers a simple approach to develop bifunctional catalytic electrodes for economically viable $H_2$ generation and sulfur recovery.

## Introduction

The fossil fuels consumption and environmental deterioration have led to growing demand for sustainable and clean energy sources.[1,2] As a leading clean energy, hydrogen ($H_2$) possesses the advantages of high energy density and environmental benign, which is crucial for future energy transition.[3] The traditional $H_2$ production ways are faced with many problems, such as serious environmental pollution, complicated equipment processes and large investment/operation expense. In comparison, the electrocatalytic overall water splitting (OWS) powered by renewable energy is a promising technology to generate high-purity $H_2$ because of mild operating conditions and simplicity.[4,5] However, this technology suffers from high voltages and costly electricity expense owing to the presence of sluggish oxygen evolution reaction (OER) at the anode, giving rise to heightened energy consumption.[6,7] At present, precious-metal-based materials including Pt/C, $RuO_2$ and $IrO_2$ are excellent materials to achieve low energy expenditure, and low reserves and high cost hinder their commercialization.[8-10] Therefore, it is appealing to exploit high-efficiency electrocatalytic systems and cheap catalysts.

Currently, researchers have adopted hybrid water electrolysis (HWE) by employing thermodynamically favorable oxidation reactions of small molecules including methanol, glycerol, urea, 5-hydroxymethylfurfural (HMF), and hydrazine, *etc*. to substitute OER at the anode, leading to optimized catalytic systems and reduced energy consumption.[11-13] Wang *et al.* prepared oxygen vacancy-riched $Co_3O_4$ and coupled the catalytic oxidation of HMF with the hydrogen evolution reaction (HER) to produce FDCA and $H_2$ at low voltages.[14] Similarly, duan *et al.* reported Au/CoOOH catalyst, which catalytically convert benzyl alcohol into high value-added products along with energy-saving $H_2$ production.[15] Among these alternative reactions, the sulfion oxidation reaction (SOR, $S^{2-} = S + 2e^-$, -0.48 V *vs.* RHE) has thermodynamic advantage.[16,17] Meanwhile, the toxic sulfion-containing wastewater is common in many industrial processes, adverse to human health and ecological environment. Therefore, combining the SOR with HER can achieve simultaneous low-voltage $H_2$ generation and degradation/conversion of sulfur-rich sewage to value-added sulfur without adding other oxidants.[18,19]

As we know, the formation and conversion of polysulfide intermediates is accompanied by a sixteen-electron transfer process during the SOR, generating slowly catalytic kinetics.[20,21] Meanwhile, the sulfur species are easy to poison metallic catalysts, greatly reducing their activities and stabilities. To resolve these challenges, researchers have engaged diverse strategies such as heteroatoms doping and constructing heterostructures *etc*. to regulate electronic structure and reduce reaction energy barriers, realizing high catalytic performances.[22-25] However, most prepared catalysts display monofunctional catalytic performances for either SOR or HER, which

---

[a] *School of Textile and Clothing, Nantong University, Nantong 226019, PR China. E-mail: liruiqing@ntu.edu.cn; zhangwei@ntu.edu.cn*
[b] *College of Food and Biological Engineering, Chengdu University, Chengdu 610106, China
E-mail: zoulonghua@cdu.edu.cn*

[1] These authors contributed equally to this work.

† Footnotes relating to the title and/or authors should appear here.

Electronic Supplementary Information (ESI) available: [details of any supplementary information available should be included here]. See DOI: 10.1039/x0xx00000x

View Article Online
DOI: 10.1039/D5SC01884F

can lead to the incompatiblility and deterioration of catalysts and high preparation cost when pairing them in the electrolytic cell. Therefore, relevant studies of bifunctional catalysts for both HER and SOR to achieve $H_2$ production are of great significance.

Herein, we develop hierarchical and efficient bimetallic selenide (Fe-$Ni_{0.85}Se$) nanosheet arrays, which serves as a bifunctional catalyst to catalyze $H_2$ production and sulfion ion oxidation. As expected, the Fe-$Ni_{0.85}Se$ displays remarkable catalytic activities for both HER and SOR. The combined Fe-$Ni_{0.85}Se$-based hybrid water electrolyzer possesses good catalytic activity and durability, which needs a low cell voltage of 0.439 V at 10 mA $cm^{-2}$, achieving energy-efficiency $H_2$ production and sulfion upgrading to valuable sulfur. The outstanding catalytic performances of Fe-$Ni_{0.85}Se$ attribute to the regulation of composition and electronic structure, therefore promoting catalytic intermediates adsorption and decreasing the energy barriers of catalytic reactions.

## Results and discussion

### Synthesis and characterization

The preparation scheme for the Fe-$Ni_{0.85}Se$ is displayed in Fig. 1a. Initially, the hydrothermal process was adopted to synthesize NiFe layered double hydroxide (NiFe LDH) on nickel foam (NF) substrate and the corresponding phase is confirmed by the X-ray diffraction (XRD, Fig. S1). The scanning electron microscopy (SEM) images show uniform and interconnected growth of NiFe LDH nanosheets with relatively smooth surface on the NF (Fig. 1b and 1c). Subsequently, black $Ni_{0.85}Se$ and Fe-$Ni_{0.85}Se$ products are obtained by a hydrothermal selenization process and several typical diffraction peaks at 33.1, 44.6, 50.5. 59.9, 61.7 and 69.6° can be attributed to (101), (102), (110), (103), (201) and (202) lattice planes of hexagonal $Ni_{0.85}Se$ (JCPDS No. 18-0888), confirming the synthesis of $Ni_{0.85}Se$ and Fe-$Ni_{0.85}Se$ (Fig. 1d). Although the Fe-$Ni_{0.85}Se$ maintains similar nanosheet-like morphology (Fig. 1e and S2), careful observation find that the Fe-$Ni_{0.85}Se$ nanosheets are composed of many nanoparticles with diameters of about 100 nm, beneficial to expose abundant active sites and promote rapid mass transport. Transmission electron microscopy (TEM) was performed to identify the morphology of Fe-$Ni_{0.85}Se$, which further confirms its nanosheet structure with composing of nanoparticles (Fig. 1f). In high-resolution TEM (HRTEM)

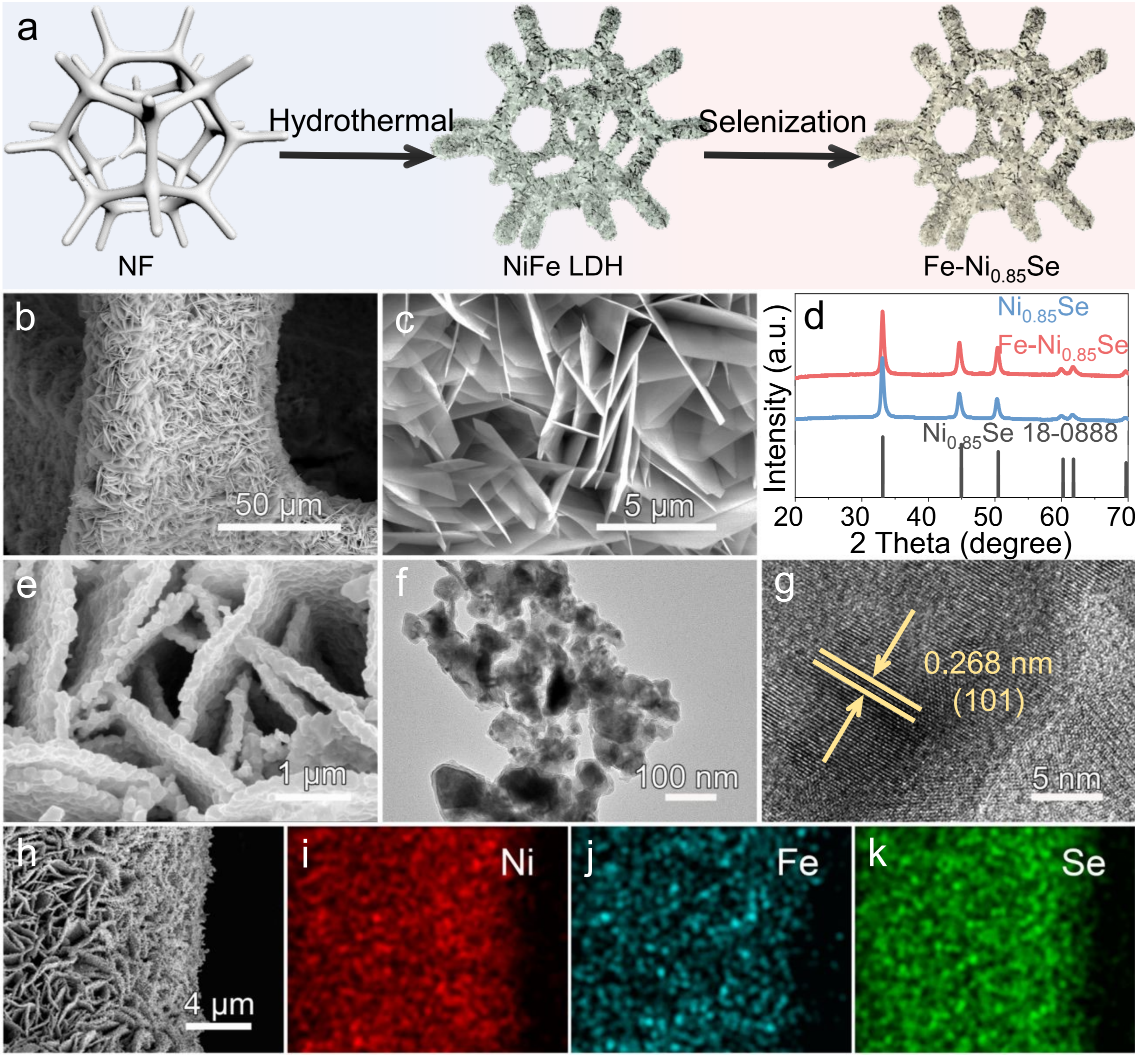

**Fig. 1** (a) Schematic diagram of preparing Fe-$Ni_{0.85}Se$. (b,c) SEM images of NiFe LDH nanosheets. (d) XRD patterns, (e) SEM, (f) TEM, (g) HRTEM, (h-k) SEM and homologous element mapping images of Fe-$Ni_{0.85}Se$.

View Article Online
DOI: 10.1039/D5SC01884F

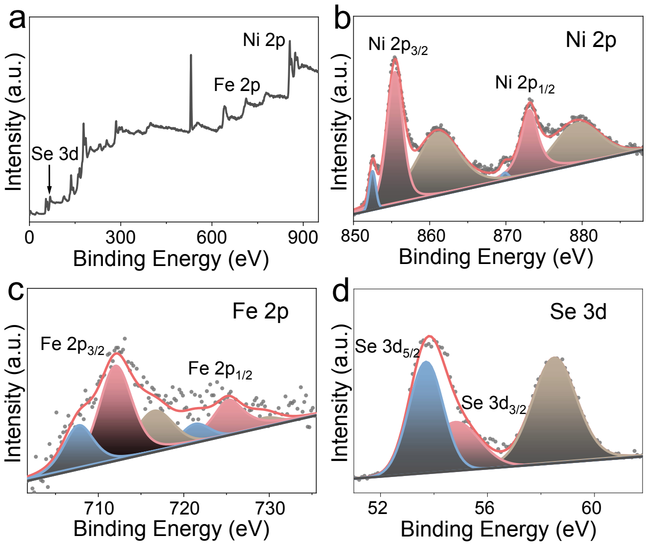

**Fig. 2** (a) Survey XPS, (b) Ni 2p, (c) Fe 2p and (d) Se 3d spectra of Fe-$Ni_{0.85}Se$.

image (Fig. 1g), an interplanar spacing of 0.268 nm attributes to the (101) crystal plane of Fe-$Ni_{0.85}Se$. The elemental mapping images (Fig. 1h-1k) reveal the existence of Ni, Fe and Se elements, which are uniformly distributed on the surface of Fe-$Ni_{0.85}Se$ nanosheets.

X-ray photoelectron spectroscope (XPS) tests were carried out to detect surface chemistry states. In Fig. 2a, survey XPS spectrum confirms the coexistence of Ni, Fe and Se elements in the Fe-$Ni_{0.85}Se$ sample. Fig. 2b displays high-resolution Ni 2p spectrum of Fe-$Ni_{0.85}Se$ and two peaks located at 852.5 and 869.9 eV are belonged to Ni $2p_{3/2}$ and Ni $2p_{1/2}$ of $Ni^{2+}$, and the binding energies at 855.5 and 873.1 eV are indexed to the Ni $2p_{3/2}$ and Ni $2p_{1/2}$ of $Ni^{3+}$.[26] The remaining two peaks at 861.1 and 879.4 eV are ascribed to satellite peaks. Likewise, the Fe 2p spectrum (Fig. 2c) shows three pairs of $2p_{3/2}/2p_{1/2}$ doublet peaks located at 707.8/721.5, 712.0/725.3 and 716.6/729.7 eV, respectively.[27] For Se species, the Se 3d spectrum of Fe-$Ni_{0.85}Se$ (Fig. 2d) is deconvoluted into two peaks at 53.7 and 54.8 eV, which are attributed to Se $3d_{5/2}$ and Se $3d_{3/2}$, indicating the presence of metal-Se bond. The peak at 58.5 eV is regarded as Se-O bond, ascribed to unavoidably slight surface oxidation.[28]

### Electrochemical performances

The HER performances of Fe-$Ni_{0.85}Se$ were assessed in the three-electrode system. In Fig. 3a and 3g, the Fe-$Ni_{0.85}Se$ displays excellent HER activity, which requires small overpotentials of 114 and 365 mV to deliver current densities of 10 and 400 mA $cm^{-2}$, lower than those of $Ni_{0.85}Se$ (138 and 411 mV), confirming the crucial role of Fe introduction on the $Ni_{0.85}Se$. The catalytic activities of Fe-$Ni_{0.85}Se$ also surpasses many developed HER catalysts (Fig. 3d and Table S1).

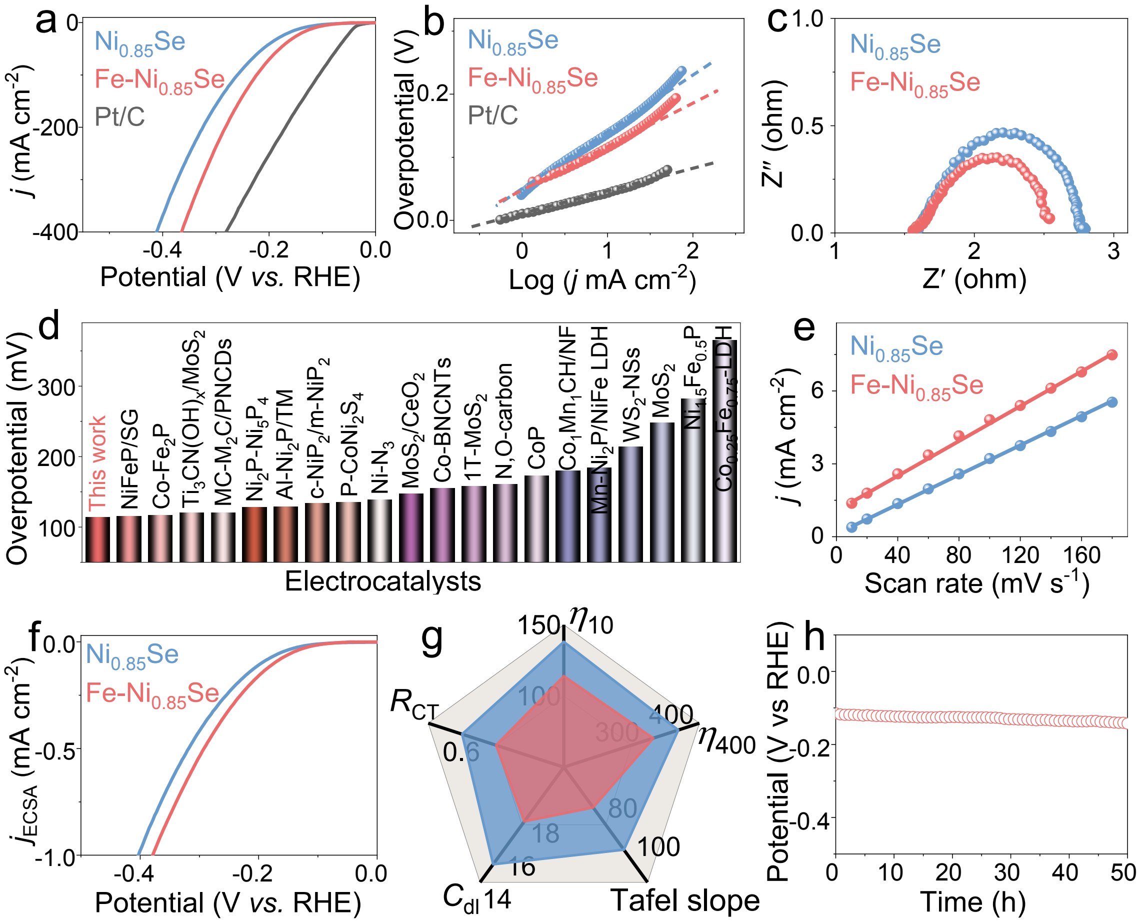

**Fig. 3** (a) HER polarization curves and (b) corresponding Tafel slopes of various catalysts. (c) EIS plots and (d) overpotentials comparison with recently developed catalysts for Fe-$Ni_{0.85}Se$. (e) $C_{dl}$ values and (f) ECSA-normalized polarization curves of $Ni_{0.85}Se$ and Fe-$Ni_{0.85}Se$. (g) HER performances radar chart. (h) Durability test of Fe-$Ni_{0.85}Se$.

Tafel plots were fitted from corresponding polarization curves to investigate HER kinetics. The Fe-$Ni_{0.85}Se$ possesses a small Tafel slope of 71 mV $dec^{-1}$ (Fig. 3b and 3g), smaller than that of $Ni_{0.85}Se$ (93 mV $dec^{-1}$), implying that the HER process of Fe-$Ni_{0.85}Se$ follows a Volmer-Heyrovsky pathway. A low Tafel slope for Fe-$Ni_{0.85}Se$ suggests that it has quick HER kinetics and outstanding catalytic activities because of the electronic structure optimization of $Ni_{0.85}Se$ after Fe doping.[29,30] To deeply understand the origin of high intrinsic activities for Fe-$Ni_{0.85}Se$, the electrochemical impedance spectroscopy (EIS) was performed. In Fig. 3c and 3g, the Nyquist plots show that the Fe-$Ni_{0.85}Se$ has smaller charge-transfer resistance ($R_{ct}$, 0.5 Ω) than that of $Ni_{0.85}Se$ (0.6 Ω), implying the key role of Fe doping in promoting charge transfer rate. Furthermore, the number of catalytic sites for Fe-$Ni_{0.85}Se$ can be quantitated by electrochemically active surface area (ECSA) derived from electrochemical double-layer capacitance ($C_{dl}$), which is calculated from cyclic voltammograms (Figs. S3). In Fig. 3e and 3g, the calculated $C_{dl}$ and ECSA values of Fe-$Ni_{0.85}Se$ (17.7 mF $cm^{-2}$ and 442.5 $cm^{-2}$) are higher than those of $Ni_{0.85}Se$ (15.1 mF $cm^{-2}$ and 377.5 $cm^{-2}$), indicating that the Fe-$Ni_{0.85}Se$ owns more abundant catalytic sites compared with $Ni_{0.85}Se$, agreeing with remarkable activity of Fe-$Ni_{0.85}Se$.[31] In Fig. 3f, the ECSA-normalized curves further reveal that the Fe-$Ni_{0.85}Se$ still has higher catalytic performances than the $Ni_{0.85}Se$, indicating that Fe doping can effectively improve intrinsic activity of $Ni_{0.85}Se$ and expose more catalytic sites. Besides, the long- term stability is a key parameter for catalysts. In Figs. 3h the chronopotentiometry (v-t) curve displays that the Fe-$Ni_{0.85}Se$ has outstanding durability without almost unchanged potentials during a 50 h of test. Moreover, the nanosheet-like morphology of Fe-$Ni_{0.85}Se$ do not change greatly (Figs. S4), and the Ni, Fe and Se elements are homogeneously distributed on the surface of Fe-$Ni_{0.85}Se$ nanosheets (Figs. S5), indicating its outstanding structural stability.

The OER performances of Fe-$Ni_{0.85}Se$ were further measured. In Fig. 4a, the Fe-$Ni_{0.85}Se$ displays good OER activities, which require small potentials of 1.485 and 1.577 mV to deliver 50 and 400 mA $cm^{-2}$, much lower than those of $Ni_{0.85}Se$ (1.536 and 1.694 mV) and $RuO_2$ (1.538 and 1.786 mV). Even so, the OER potentials for Fe-$Ni_{0.85}Se$ are still high, leading to high energy consumption when coupling with the HER. Therefore, it is promising to replace OER with SOR to lower anode potentials and achieve energy-efficient $H_2$ production. The SOR activities were evaluated in 1 M NaOH containing various concentrations of $Na_2S$ (0.5-1.5 M). The SOR activity of Fe-$Ni_{0.85}Se$ rapidly increases when the concentration of $Na_2S$ raises to 1 M (Figure S6). In 1 M NaOH containing 1 M $Na_2S$, the Fe-$Ni_{0.85}Se$ displays splendid SOR activities with low potentials of 0.340 and 0.593 V at 10 and 400 mA $cm^{-2}$ (Fig. 4b and 4d), smaller than those of $Ni_{0.85}Se$ (0.372 and 0.635 V), $RuO_2$ (0.406 and 0.893 V) and most previously developed SOR materials (Table S2). Moreover, the SOR process of Fe-$Ni_{0.85}Se$ shows greatly reduced potentials compared with the OER, confirming the feasibility of replacing the OER with SOR to realize low cell voltages. The corresponding Tafel plots (Fig. 4c) manifest that the Fe-$Ni_{0.85}Se$ still possesses smaller Tafel slope value (81 mV $dec^{-1}$) than that of $Ni_{0.85}Se$ (104 mV $dec^{-1}$) and $RuO_2$ (179 mV $dec^{-1}$), implying that the Fe-$Ni_{0.85}Se$ has fast SOR kinetics.[32] The stability of Fe-$Ni_{0.85}Se$ was also conducted. In Fig. 4e, the Fe-$Ni_{0.85}Se$ reveals almost constant potentials over a 20 h of test and the corresponding nanosheet-like morphology (Fig. S7) and homogeneous distribution of Ni, Fe and Se elements are well maintained (Fig. S8), further illustrating its good durability for SOR.

Motivated by eminent HER and SOR performances of Fe-$Ni_{0.85}Se$ (Fig. 5a), traditional and hybrid two-electrode electrolyzers were assembled. In Fig. 5b, the HWE electrolyzer can output current densities of 10 and 200 mA $cm^{-2}$ at small cell voltages ($V_{10}$, and $V_{200}$) of 0.439 and 0.811 V, smaller than those needed in conventional OWS system (1.625 and 1.998 V). In Fig. 5c, the stability test curve shows that the Fe-$Ni_{0.85}Se$ operates steadily for 100 h with negligible voltages degradation, confirming its outstanding durability. After the durability test, the relevant electrolyte is acidified by sulfuric acid and yellow powders are obtained, which are verified to elemental sulfur

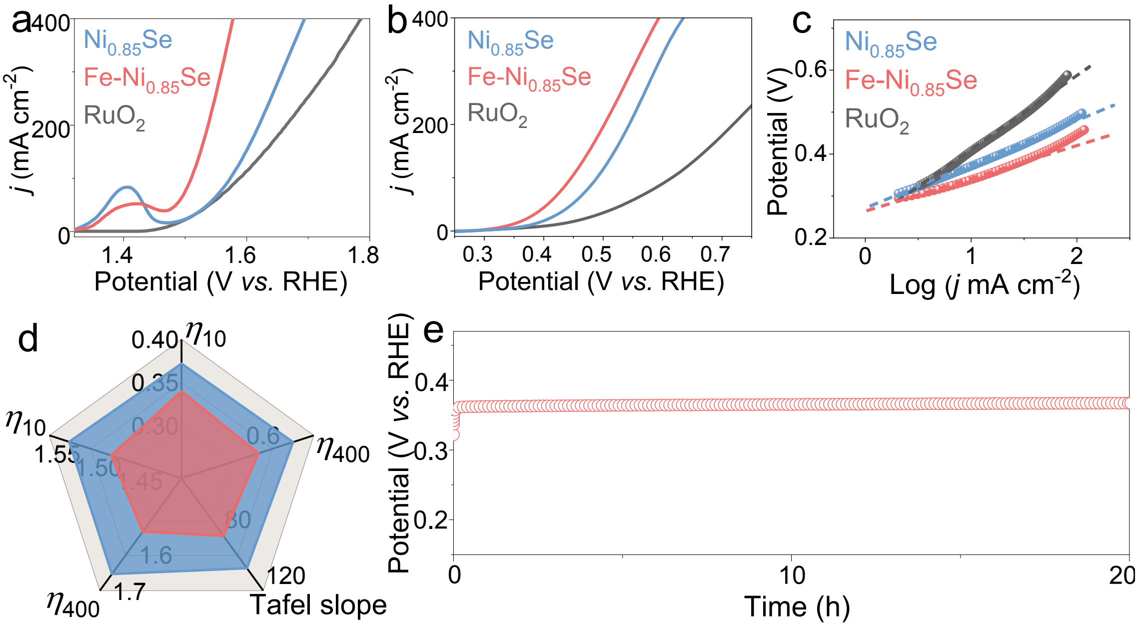

**Fig. 4** Polarization curves of (a) OER, (b) SOR and (c) Tafel slopes for catalysts. (d) OER and SOR performances radar chart of $Ni_{0.85}Se$ and Fe-$Ni_{0.85}Se$. (e) Stability measurement of Fe-$Ni_{0.85}Se$.

View Article Online
DOI: 10.1039/D5SC01884F

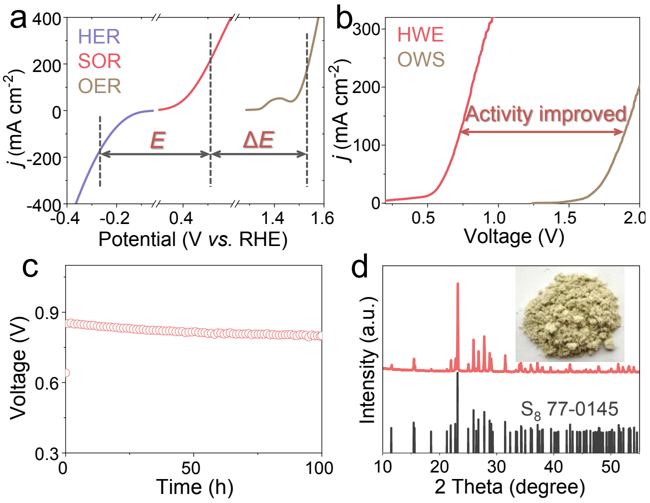

**Fig. 5** (a) Voltage difference between HER and SOR/OER and (b) polarization curves of HWE and OWS systems for Fe-$Ni_{0.85}Se$. (c) Durability test of HWE process. (d) XRD pattern of S product. Inset: digital image of S.

($S_8$, PDF#77-0145, Fig. 5d), implying high valuable sulfur recovery. These results indicate the substitution of OER by SOR not only significantly decrease cell voltages of $H_2$ production, but also gain high-value sulfur product in the sulfion-rich wastewater.

## Theoretical analysis

To reveal the origin of high HER and SOR performances of Fe-$Ni_{0.85}Se$, we carried out the density functional theory (DFT) simulations to illustrate their reaction mechanism. The structure models are displayed in Fig. 6a and S9. The adsorption and dissociation of $H_2O$ and free energy change of H* ($\Delta G_{H*}$) for HER are analyzed. In Fig. 6b, the Fe-$Ni_{0.85}Se$ shows lower $H_2O$ adsorption energy ($E_{H2O}$, -0.81 eV) than that of $Ni_{0.85}Se$ (-0.16 eV), indicating that the $H_2O$ molecules are easily adsorbed on the surface of Fe-$Ni_{0.85}Se$ to perform subsequent dissociation process.[33] For the $Ni_{0.85}Se$, the $H_2O$ dissociation and adsorbed hydrogen (H*) generation energy barrier are calculated to 1.36 and 1.18 eV, indicating. After the Fe doping, the corresponding energy barriers of Fe-$Ni_{0.85}Se$ reduce to 1.13 and 0.99 eV, indicating that $H_2O$ dissociation process of Fe-$Ni_{0.85}Se$ is more thermodynamically favorable to produce H* compared with the $Ni_{0.85}Se$.[34] Meanwhile, the $\Delta G_{H*}$ value of Fe-$Ni_{0.85}Se$ is calculated to 0.61 eV (Fig. 6e), which closes to thermoneutrality compared with the $Ni_{0.85}Se$ (0.77 eV), implying fast $H_2$ production capacity for Fe-$Ni_{0.85}Se$.[35] The structure models of $H_2O$ dissociation and H* on the $Ni_{0.85}Se$ and Fe-$Ni_{0.85}Se$ are displayed in Fig. S10-S12. Additionally, DFT analysis for SOR process was carried out and the intermediates energy changes of stepwise oxidation of $S^{2-}$ to $S_8$ ($S^{2-} \rightarrow S^* \rightarrow S_2^* \rightarrow S_3^* \rightarrow S_4^* \rightarrow S_8^* \rightarrow S_8$) on the $Ni_{0.85}Se$ and Fe-$Ni_{0.85}Se$ were estimated on the $Ni_{0.85}Se$ and Fe-$Ni_{0.85}Se$ (Fig. 6f and S13). Notably, the Fe-$Ni_{0.85}Se$ has a more negative energy barrier value for $S^{2-}$ ions adsorption ($\Delta G_{*S}$, -0.51 eV) compared to that of $Ni_{0.85}Se$ (-0.36 eV),

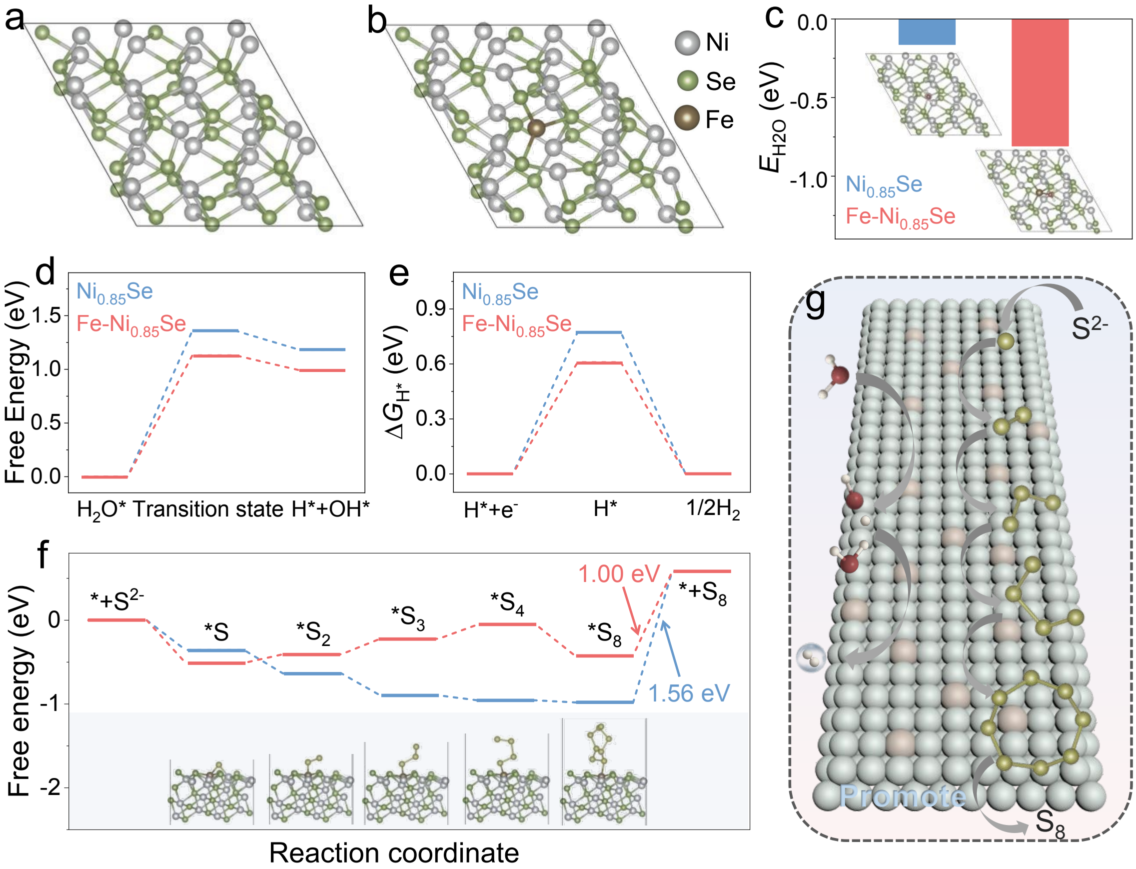

**Fig. 6** Structural models of (a) $Ni_{0.85}Se$ and (b) Fe-$Ni_{0.85}Se$. (c) Water adsorption and (d) activation energy, (e) $\Delta G_{H*}$ comparison, and (f) free energy profiles of stepwise SOR of $Ni_{0.85}Se$ and Fe-$Ni_{0.85}Se$. (g) Schematic diagram for the HER and SOR processes.

View Article Online
DOI: 10.1039/D5SC01884F

implying a favorable $S^{2-}$ adsorption for Fe-$Ni_{0.85}Se$, which is vital for subsequent desulfurization process.[36,37] According to calculated free energy changes (Fig. 6f), the desorption process of $*S_8$ to $S_8$ is identified as rate determining step (RDS) for $Ni_{0.85}Se$, requiring a high energy barrier of 1.56 eV. After doping the Fe, the Fe-$Ni_{0.85}Se$ needs a small free energy barrier of 1.00 eV for desorbing, $*S_8$ to $S_8$, which effectively increases SOR performances. These results indicate that the Fe introduction not only promotes water dissociation and optimizes thermodynamic efficiency of H* during the HER, but also speeds up the oxidation process of $S^{2-}$ for the SOR, consistent with above high HER and SOR performances of Fe-$Ni_{0.85}Se$.

## Conclusions

In summary, we constructed a Fe-$Ni_{0.85}Se$ catalyst *via* hydrothermal and selenization strategies, which reveals splendid catalytic activities towards HER and SOR in alkaline electrolyte due to the synergistic effect of Fe incorporation and uniform nanosheet arrays. The resultant Fe-$Ni_{0.85}Se$ outputs 10 mA $cm^{-2}$ with a small overpotential of 114 mV for HER and potential of 0.340 V for SOR. Meanwhile, the assembled Fe-$Ni_{0.85}Se$-based electrolyzer achieves energy-saving $H_2$ generation and sulfion upgrading to value-added sulfur product, which needs low cell voltages of 0.439 and 0.811 V to reach 10 and 200 mA $cm^{-2}$. DFT calculations reveal that the Fe incorporation plays vital roles in increasing HER and SOR performances, which can enhance the adsorption of catalytic reactants and intermediates and lower energy barriers for HER and SOR. This study offers a new scheme for efficient preparation of $H_2$ and sulfur in the sulfion-containing wastewater.

## Data availability

The relevant experimental and characterization data are available in the article and the ESI.

## Author Contributions

Shuixiang Xie: Data curation, Formal analysis. Xiaojun Wang: Data curation, Formal analysis. Yuhuan Li: Investigation. Shijie Liu: Formal analysis. Jiahui Qian, Investigation. Yuhan Zhang: Data curation. Linling Jiang: Data curation. Zhe Cao: Formal analysis. Zhenhao Yan: Investigation. Xiaoyu Wan: Writing-review & editing. Zhaohang Yang: Investigation. Longhua Zou: Software. Wei Zhang: Conceptualization, writing-review & editing. Rui-Qing Li: Conceptualization, writing-review & editing.

## Conflicts of interest

There are no conflicts to declare.

## Acknowledgements

This work is financially supported by the National Natural Science Foundation of China (No. 22302103), the Natural Science Foundation of Jiangsu Province (No. BK20230619), the Natural Science Foundation of the Jiangsu Higher Education Institutions of China (No. 23KJB540003), the Natural Science Foundation of Nantong Municipality (No. JC2023015), the Opening Project of Key Laboratory of Advanced Electrode Materials for Novel Solar Cells for Petroleum and Chemical Industry of China, Suzhou University of Science and Technology (No. 2024A038), the Postgraduate Research & Practice Innovation Program of Jiangsu Province (No. KYCX25_3762), the College Students Innovation and Entrepreneurship Training Program, and the Large Instruments Open Foundation of Nantong University (No. KFJN2457). The authors also thank the help from Ceshigo Research Service (www.ceshigo.com) for theoretical calculation and the Nantong University Analysis and Testing Center for the technical support.

## Notes and references

1 J. Turner, *Science*, 2022, **376**, 1361.
2 P. Shi, J. Li, Y. Song, N. Xu, J. Zhu, *Nano Lett.*, 2024, **24**, 5673.
3 X. Zhou, J. Zhang, M. Zhang, X. Du, W. Bao, J. Han, X. Lin, P. Zhang and Z. Luo, *Inorg. Chem. Front.*, 2025, **12**, 10.1039/D5QI00418G.
4 Y. Wu, M. Chen, H. Sun, T. Zhou, X. Chen, G. Na, G. Qiu, D. Li, N. Yang, H. Zheng, Y. Chen, B. Wang, J. Zhao, Y. Zhang, J. Zhang, F. Liu, H. Cui, T. He and Q. Liu, *Appl. Catal. B*, 2025, **360**, 124548.
5 X. Deng, X. Zheng, Z. Gong, W. Tan and X. Pei, *Chin. J. Rare Met.*, 2023, **47**, 43.
6 R. Li, S. Guo, X. Wang, X. Wan, S. Xie, Y. Liu, C. Wang, G. Zhang, J. Cao, J. Dai, M. Ge and W. Zhang, *Chem. Sci.*, 2024, **15**, 10084.
7 C. Walter, P. Menezes and M. Driess, *Chem. Sci.*, 2021, **12**, 8603.
8 Y. Wu, M. Chen, D. Liu, H. Sun, T. Zhou, G. Na, G. Qiu, D. Li, Y. Chen, J. Zhao, Y. Zhang, J. Zhang, H. Pan, F. Liu, H. Cui and Q. Liu, *J. Mater. Sci. Technol.*, 2025, **215**, 111.
9 Y. Wang, S. Wang, Z. Ma, L. Yan, X. Zhao, Y. Xue, J. Huo, X. Yuan, S. Li and Q. Zhai, *Adv. Mater.*, 2022, **34**, 2107488.
10 D. Li, M. Chen, D. Liu, C. Shen, H. Sun, Y. Zhang, T. He, Q. Lu, B. Li, T. Zhou, B. Wang, Y. Wu, G. Na, Y. Chen, J. Zhao, Y. Zhang, J. Zhang, F. Liu, H. Cui and Q. Liu, *Adv. Energy Mater.*, 2024, **15**, 2404714.
11 P. Zhu, M. Shi, Z. Shen, X. Liao and Y. Chen, *Chem. Sci.*, 2024, **15**, 4723.
12 P. Zhou, X. Lv, S. Tao, J. Wu, H. Wang, X. Wei, T. Wang, B. Zhou, Y. Lu, T. Frauenheim, X. Fu, S. Wang and Y. Zou, *Adv. Mater.*, 2022, **34**, 2204089.
13 R. Li, S. Zeng, B. Sang, C. Xue, K. Qu, Y. Zhang, W. Zhang, G. Zhang, X. Liu, J. Deng, O. Fontaine and Y. Zhu, *Nano Res.*, 2023, **16**, 2543.
14 Y. Lu, T. Liu, C. Dong, C. Yang, L. Zhou, Y. Huang, Y. Li, B. Zhou, Y. Zou and S. Wang, *Adv. Mater.*, 2022, **34**, 2107185.
15 Z. Li, Y. Yan, S. Xu, H. Zhou, M. Xu, L. Ma, M. Shao, X. Kong, B. Wang, L. Zheng and H. Duan, *Nat. Commun.*, 2022, **13**, 147.
16 L. Zhang, Z. Wang and J. Qiu, *Adv. Mater.*, 2022, **34**, 2109321.
17 W. Wang, Q. Mao, S. Jiang, K. Deng, H. Yu, Z. Wang, Y. Xu, L. Wang and H. Wang, *Appl. Catal. B-Environ.*, 2024, **340**, 123194.
18 R. Li, X. Wang, S. Xie, S. Guo, Z. Cao, Z. Yan, W. Zhang and X. Wan, *Chem. Sci.*, 2025, **16**, 809.
19 H. Wang, H. Yao, Q. Guo and H. Xia, *J. Nantong Univ.(Nat. Sci. Ed.)*, 2024, **23**, 45.
20 L. Yi, Y. Ji, P. Shao, J. Chen, J. Li, H. Li, K. Chen, X. Peng and Z. Wen, *Angew. Chem. Int. Ed.*, 2021, **60**, 21550.
21 Y. Pei, D. Li, C. Qiu, L. Yan, Z. Li, Z. Yu, W. Fang, Y. Lu and B. Zhang, *Angew. Chem. Int. Ed.*, 2024, **63**, e202411977.

View Article Online
DOI: 10.1039/D5SC01884F

22 R. Li, X. Xu, J. Zeng, X. Zhang, X. Wan, S. Guo, X. Wang, S. Xie, Z. Cao, Y. Zhang, C. Wang, J. Deng, O. Fontaine, M. Ge, J. Dai, G. Zhang, W. Zhang, X. Wang and Y. Zhu, *Nano Lett.*, 2025, **25**, 1272.

23 R. Xu and Z. Wang, *J. Nantong Univ.(Nat. Sci. Ed.)*, 2024, **23**, 21.

24 T. Xue, Z. Huang, H. Gu and H. Zhang. *Chin. J. Rare Met.*, 2024, **48**, 90.

25 R. Li, H. Su, S. Xie, X. Wan, C. Wang, G. Zhang, M. Ge, J. Dai, C. Xue, C. Li, J. Cao and W. Zhang, *Rare Met.*, 2024, **43**, 6426.

26 H. Yan, Y. Xie, A. Wu, Z. Cai, L. Wang, C. Tian, X. Zhang and H. Fu, *Adv. Mater.*, 2019, **31**, 1901174.

27 C. Lyu, Y. Li, J. Cheng, Y. Yang, K. Wu, J. Wu, H. Wang, W. Lau, Z. Tian, N. Wang and J. Zheng, *Small*, 2023, **19**, 2302055.

28 Y. Chang, P. Zhai, J. Hou, J. Zhao and J. Gao, *Adv. Energy Mater.*, 2022, **12**, 2102359.

29 X. Du, J. Zhang, X. Zhou, M. Zhang, N. Wang, X. Lin, P. Zhang, and Z. Luo, *Green Chem.*, 2025, **27**, 3515.

30 H. Luo, L. Li, F. Lin, Q. Zhang, K. Wang, D. Wang, L. Gu, M. Luo, F. Lv and S. Guo, *Adv. Mater.*, 2024, **36**, 2403674.

31 H. Ding, C. Su, J. Wu, H. Lv, Y. Tan, X. Tai, W. Wang, T. Zhou, Y. Lin, W. Chu, X. Wu, Y. Xie and C. Wu, *J. Am. Chem. Soc.*, 2024, **146**, 7858.

32 H. Yu, W. Wang, Q. Mao, K. Deng, Y. Xu, Z. Wang, X. Li, H. Wang and L. Wang, *J. Mater. Chem. A*, 2023, **11**, 2218.

33 Y. Hu, L. Shao, Z. Jiang, L. Shi, Q. Li, K. Shu, H. Chen, G. Li, Y. Dong, T. Wang, J. Li, L. Jiao and Y. Deng, *Adv. Funct. Mater.*, 2024, **34**, 2411011.

34 Q. Zhou, H. Hu, Z. Chen, Xiao Ren and D. Ma, *Chem. Sci.*, 2025, **16**, 1597.

35 T. Wang, L. Miao, S. Zheng, H. Qin, X. Cao, L. Yang, and L. Jiao, *ACS Catal.*, 2023, **13**, 4091.

36 Y. Pei, D. Li, C. Qiu, L. Yan, Z. Li, Z. Yu, W. Fang, Y. Lu and B. Zhang, *Angew. Chem. Int. Ed.*, 2024, **63**, e202411977.

37 D. He, P. Yang, K. Yang, J. Qiu and Z. Wang, *Adv. Funct. Mater.*, 2024, **34**, 2407601.

View Article Online
DOI: 10.1039/D5SC01884F

## Data availability

The relevant experimental and characterization data are available in the article and the ESI.